Vectorial modal analysis of dielectric waveguides based on a coupled transverse-mode integral equation. I. Mathematical formulation

Hung-Wen Chang and Tso-Lun Wu

Institute of Electro-optical Engineering, National Sun Yat-sen University, Kaohsiung, 80424 Taiwan

Meng-Huei Sheng

Department of Management Information Science, Chia Nan University of Pharmacy & Science, Tainan, 71710 Taiwan

Received August 26, 2005; revised December 4, 2005; accepted December 8, 2005; posted January 3, 2006 (Doc. ID 64404)

We propose a rigorous full-vector integral-equation formulation for analyzing modal characteristics of the complex, two-dimensional, rectangular-like dielectric waveguide that is divisible into vertical slices of one-dimensional layered structures. The entire electromagnetic mode field is completely determined by the y-component electric and magnetic field functions on the interfaces between slices. These interfacial functions are governed by a system of vector-coupled transverse-mode integral equations (VCTMIE) whose kernels are made of orthonormal sets of both TE-to-y and TM-to-y modes from each slice. To solve for the unknown functions, we construct sets of suitable expansion functions and turn VCTMIE into a nonlinear matrix equation via orthogonal projection. The eigenvectors of the matrix provide the mode field solutions of the complex dielectric waveguide.

OCIS codes: 000.3860, 000.4430, 130.0130, 230.4170, 230.7370.

1. INTRODUCTION

Integrated dielectric waveguides are one of the critical passive optical components used in modern communication systems. To reduce costs and to shorten the product development cycle, it is crucial to be able to compute accurately the propagation constants β as well as the electromagnetic field profiles of these complex optical devices so that the devices will perform as intended. Although waveguide propagation constants can be very accurately computed, accurate two-dimensional (2D) vector field solutions are harder to compute, especially when there are degenerate modes with similar β values. Unlike microwave waveguide problems, which can be divided into uncoupled TE and TM cases, a 2D, rectangular-pattern dielectric waveguide (RWG) has all six EM components simultaneously present inside the waveguide. The TE and TM modes are coupled in the RWG making it difficult to find the vector field solutions of various orders.

There are many published techniques for the analysis of the general dielectric waveguide. The simplest, yet practical ways are the effective-index method and its variations.[1–4] They provide easy and fast calculation of the waveguide propagation constants but are not designed to compute the mode field distribution. More elaborate techniques have been developed for finding the fields. The long list includes the point-matching method,[5] mode-matching technique,[6] equivalent network method,[7] combination of volume integral equation (IE) with method of moment constructed on top of various basis functions,[8–13] method of line,[14,15] and film mode matching (FMM).[16,17] For complex but compact optical devices, techniques such as the frequency-domain-finite-difference (FD-FD) and finite-element (FE) methods can be quite effective. For extremely large optical structures with smoothly changing index profiles such as adiabatic waveguides, the beam-propagation method (BPM) and its variations are extensively used for field evolutions and mode profile determination. BPM methods apply a one-way approximation to Maxwell's equations making it possible to advance the field solutions plane by plane along the propagation axis. For detailed discussions of these techniques, please refer to an excellent review paper by Scarmozzino *et al.*[15]

Some of the full-vector techniques are capable of providing modal analysis of RWGs such as ridged waveguides; each has its advantages and limitations. For example, the FD-FD and FE methods are built on transverse E-field coupled partial differential equations of E_x and E_y components or H-field H_x and H_y components. The differential operators are approximated by finite-difference approximations together with clever index averaging to reduce the sampling resolution. Thus, they can handle complex waveguide geometry with graded or step index profiles. The unknowns on the FD grid points, as well as the FE cells, satisfy a set of simultaneously linear equations with the matrix coefficients depending on the propagation constant. Nontrivial solutions, which are the eigenvectors of the matrix (in the null space), are the desired modal solutions; they exist only for certain propagation constants. This leads to a nonlinear eigenvalue eigenvector problem which, due to its massive size, cannot be solved by the direct method and must rely on converging iterative methods for searching propagation constants

and mode field solutions. It is interesting that some vectorial BPM methods use similar techniques to analyze complex waveguide modes. Finite-difference time-domain (FDTD) methods use all six EM components to simulate the time evolution of three-dimensional (3D) vector fields that are due to initial field distribution or to given EM sources. Based on a staggered space–time grid system, it has the advantage in that time stepping of the EM fields can be computed directly without solving any matrix equation. Thus the FDTD method is often used to obtain field solutions of single-mode waveguides.

We present here, in essence, a generalization of the FMM method. It is based on a full-vector coupled transverse-mode integral-equation (VCTMIE) formulation to compute accurately multiple waveguide modes of RWGs. Like FMM, it employs both TE-to-y and TM-to-y modes and the mode-matching principle to determine RWG modes. This paper is divided into two parts. This part, part I, treats the background information and theoretical formulation of the general 2D RWG. Part II[18] deals with the numerical aspect such as the algorithm implementation and waveguide examples.

2. THEORY

The general RWG optical waveguide is shown in Fig. 1. The original structure is divided into sections by a series of vertical divisions. Each section, called a slice, is then approximated by horizontal, parallel dielectric layers. There are altogether $(M+1)$ slices and M vertical interfaces between these slices. The formulation allows different boundary conditions (BCs), such as Dirichlet's BCs, Neumann's BCs, or Sommerfeld radiation conditions, at both the left and right sides of this structure. To construct orthogonal slice modes, we place two perfectly electric/magnetic conducting walls (PCWs) at both the upper and lower boundaries. Although an exact integral equation formulation can still be obtained if we remove the two artificial PCWs, it would be quite difficult to solve the equation numerically, and we will elaborate more on this in Subsection 3.C.

Normally there are two independent electromagnetic field solutions called TE and TM modes in a hollow microwave waveguide with E_z and H_z as root components. All the other electromagnetic fields can be derived from these two components. In the cylindrical coordinate system, it is the conventional procedure to classify the modes as E_z (TM-to-z) and H_z (TE-to-z) components for the fiber optics theory, because these are the only components satisfying the scalar Helmholtz equation. For our RWGs made of slices of dielectric layers, all six Cartesian components satisfy the scalar Helmholtz equation. Within each slice, we wish to find the simplest vector modal representation derived from a single scalar potential. The fields E_z and H_z are not the best choices since they are coupled in each slice. Fortunately, it is known that the normal field components D_y and B_y are two independent solutions within each slice. Here we name the solutions the TE-to-y and TM-to-y modes according to Harrington's book.[19] They are also associated with modes generated from the y-component electric and magnetic Hertz vectors,[20] respectively. Modal formulation based on D_y and B_y can be found in Refs. 21 and 22. They are the only scalar components needed to generate all five other components in the TM-to-y and TE-to-y modes.

The independent D_y and B_y are, however, coupled along the boundary between two slices. At the interface across two neighboring slices, the tangential vertical field components E_y and H_y are required to be continuous. Later in the paper we show that these unknown interfacial field

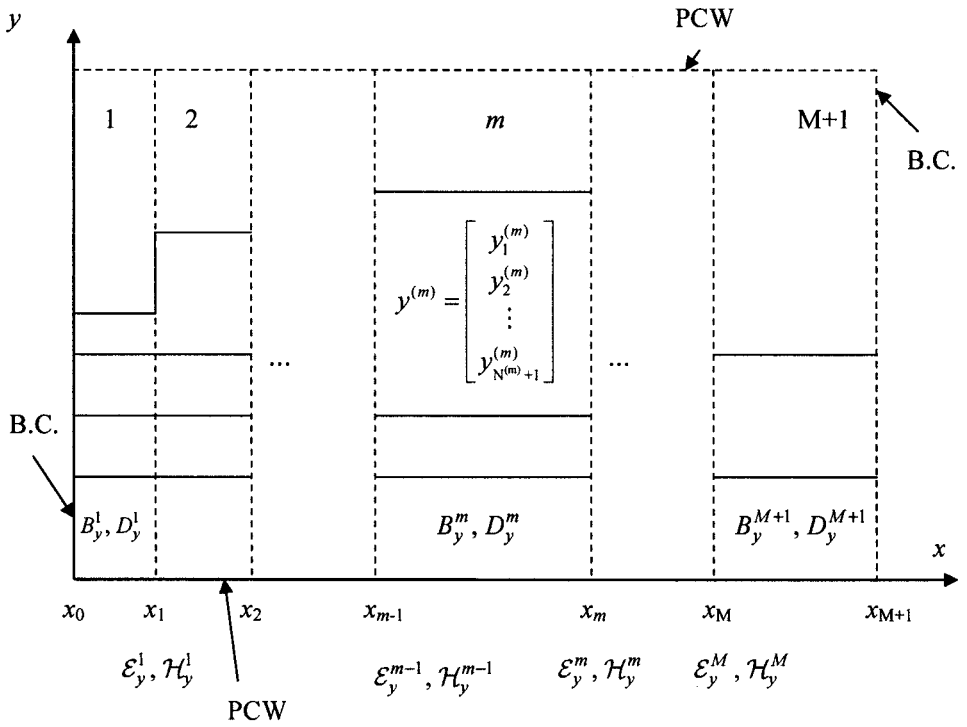

Fig. 1. General RWG divided into $(M+1)$ regions (slices) made of layered dielectric waveguide.

Table 1. Notation and Symbols

Symbols and Subscripts	Description
ϕ, ψ	Basis functions
Φ, Ψ	Derivatives of basis functions
$\mathbf{P},\mathbf{Q},\mathbf{R},\mathbf{S},\mathbf{A},\mathbf{T}$	Matrices
$\mathbb{G},\mathbb{P},\mathbb{Q},\mathbb{R},\mathbb{S}$	Kernals of operators
$E,H,D,B,\mathcal{E},\mathcal{H}$	EM fields
$\mathbf{F}$	Vector field functions
m,n	Mode (region, interface) pointers
l,r	Left or right indicators
B,D	Normal continuous EM components
e,h	Tangential EM components
x,y,z	Direction indicators
M,N	Total slice interfaces, total slice modes
N_b	Total basis modes

functions, denoted by the calligraphic $\mathcal{E}(y)$ and $\mathcal{H}(y)$ symbols, are crucial in our analysis. For any particular slice, we can determine the unknown coefficients of the two independent layer modes generated from D_y and B_y using the two adjacent pairs of $\mathcal{E}(y)$ and $\mathcal{H}(y)$. The tangential $E_z(y)$ and $H_z(y)$ components can then be generated on the slice boundaries. The continuity of these z-component functions will lead to coupled integral equations for all these $\mathcal{E}(y)$ and $\mathcal{H}(y)$ functions on all M interfaces.

We shall denote the equation for RWGs as VCTMIE, defined above. The simplest TMIE formulation for studying the scattering off a periodic grating can be found in Chapter 7 of Ref. 20. The application of TMIE to the dielectric waveguide termination problems can be found in Ref. 23, in which the authors first coined the term TMIE. For a list of all symbols and notations used in the paper please refer to Table 1. Although it is a well-known fact that D_y and B_y are the mode-generating functions for h and e modes, the governing second-order differential equation and the detailed derivation into Sturm–Liouville form are hard to find in the literature. We include the analysis in Appendix A.

By writing the y-components of D_y (TM mode or e mode) and B_y (TE mode or h mode) as $\phi_D(y)\times\exp(-jk_{xD}x)\exp(-j\beta z)$ and $\phi_B(y)\exp(-jk_{xB}x)\exp(-j\beta z)$, we obtain [see Eqs. (A13a) and (A13b)] the following differential equations for the eigenfunctions $\phi_B(y)$ and $\phi_D(y)$:

$$\phi_B''(y)+k_0^2\epsilon_r(y)\phi_B(y)=\lambda_B\phi_B(y), \tag{1a}$$

$$\left[\frac{\phi_D'(y)}{\epsilon_r(y)}\right]'+k_0^2\phi_D(y)=\lambda_D\frac{\phi_D(y)}{\epsilon_r(y)}, \tag{1b}$$

where k_0 is the wavenumber in a vacuum and y-dependent $\epsilon_r(y)$ is the relative dielectric constant within each slice. The relative permeability constant μ_r is assumed to be unity. The single prime denotes the first derivative with respect to y. Here, β is the propagation constant, and the parameters k_{xD} and k_{xB} are the wavenumbers in the x direction. They are different, but remain constant in all layers for a particular combination of λ,β. The eigenvalues λ_D and λ_B and the dispersion relationships are given by Eqs. (A14). The cutoff wavenumbers k_{cD} and k_{cB} are related to λ_D and λ_B. For a particular combination of λ,β there are many k_{cD} and k_{cB} for different eigenmodes. Note that the y-direction wavenumbers, which are denoted by k_{yD} and k_{yB}, are different in all layers for a particular combination of $\lambda,\beta,\lambda_D,\lambda_B$. The process of obtaining these slice modes (or region modes) is as follows: Given the wavelength λ, we first compute a set of eigenvalues and the associated eigenfunctions. We then scan for the propagation constant for the desired waveguide mode. At each β scan, we compute k_{xB} and k_{xD} for the entire slice and $k_{yD}(y)$ and $k_{yB}(y)$ for all layers in the given slice. The complete planar expansion of all the fields can then be expressed with the three sets of wavenumbers k_x, k_y, and β.

Next, for the entire dielectric waveguide, we represent the electric flux $D_y(x,y,z)$ as the following linear combination of the plane-wave solutions:

$$D_y^{(1)}(x,y,z)=\sum_n c_{D,n}^{(1)}\phi_{D,n}^{(1)}(y)\psi_{D,n}^{(1,r)}(x)\exp(-j\beta z), \tag{2a}$$

$$D_y^{(m)}(x,y,z)=\sum_n \phi_{D,n}^{(m)}(y)[c_{D,n}^{(m,l)}\psi_{D,n}^{(m,l)}(x)+c_{D,n}^{(m,r)}\psi_{D,n}^{(m,r)}(x)]\times\exp(-j\beta z), \tag{2b}$$

$$D_y^{(M+1)}(x,y,z)=\sum_n c_{D,n}^{(M+1)}\phi_{D,n}^{(M+1)}(y)\psi_{D,n}^{(M+1,l)}(x)\exp(-j\beta z), \tag{2c}$$

and the magnetic flux $B_y(x,y,z)$ as

$$B_y^{(1)}(x,y,z)=\sum_n c_{B,n}^{(1)}\phi_{B,n}^{(1)}(y)\psi_{B,n}^{(1,r)}(x)\exp(-j\beta z), \tag{3a}$$

$$B_y^{(m)}(x,y,z)=\sum_n \phi_{B,n}^{(m)}(y)[c_{B,n}^{(m,l)}\psi_{B,n}^{(m,l)}(x)+c_{B,n}^{(m,r)}\psi_{B,n}^{(m,r)}(x)]\times\exp(-j\beta z), \tag{3b}$$

$$B_y^{M+1}(x,y,z)=\sum_n c_{B,n}^{(M+1)}\phi_{B,n}^{(M+1)}(y)\psi_{B,n}^{(M+1,l)}(x)\exp(-j\beta z). \tag{3c}$$

The unknown coefficients for the nth mode in the mth slice are denoted by $c_{D,n}^{(m)}$ and $c_{B,n}^{(m)}$, respectively, for D_y and B_y. The letters l and r in $c_{B,n}^{(m,l)}$, $\psi_{B,n}^{(m,l)}$ and $c_{B,n}^{(m,r)}$, $\psi_{B,n}^{(m,r)}$ indicate the association of the fields with the left- and right-side interfacial functions, respectively, in the mth slice. The upper limits of the above summations are assumed to be infinity and will be omitted throughout the paper. The exact definition of the x-dependent function $\psi(x)$ in the first and the last slice depends on the actual boundary conditions. For example, in the first slice, for Sommerfeld radiation conditions, it is given by

$$\psi_{F,n}^{(1,r)}(x)=\frac{\exp(k_{xF,n}^{(1)}x)}{\exp(k_{xF,n}^{(1)}x_1)}, \tag{4a}$$

and for Dirichlet's BC it is given by

$$\psi_{F,n}^{(1,r)}(x)=\frac{\sin[k_{xF,n}^{(1)}(x-x_0)]}{\sin(k_{xF,n}^{(1)}\Delta x_1)}. \tag{4b}$$

Finally, for Neumann's BC, it takes the form

$$\psi_{F,n}^{(1,r)}(x)=\frac{\cos[k_{xF,n}^{(1)}(x-x_0)]}{\cos(k_{xF,n}^{(1)}\Delta x_1)}. \tag{4c}$$

In Eqs. (4) the subscript F is used to denote either B or D. For $2\leqslant m\leqslant M$, $\psi^{(m)}(x)$ can be defined as

$$\psi_{F,n}^{(m,l)}(x)=\frac{\sin[k_{xF,n}^{(m)}(x_m-x)]}{\sin(k_{xF,n}^{(m)}\Delta x_m)}, \tag{5a}$$

$$\psi_{F,n}^{(m,r)}(x)=\frac{\sin[k_{xF,n}^{(m)}(x-x_{m-1})]}{\sin(k_{xF,n}^{(m)}\Delta x_m)}, \tag{5b}$$

where $\Delta x_m=x_m-x_{m-1}$. Note that $\psi_{F,n}^{(m,l)}(x)$ and $\psi_{F,n}^{(m,r)}(x)$ are two independent functions as long as the denominator $\sin(k_{xF,n}^{(m)}\Delta x_m)$ remains nonzero. These functions have a useful property, with $\psi_{F,n}^{(m,r)}(x_{m-1})=0$ and $\psi_{F,n}^{(m,l)}(x_{m-1})=1$ at $x=x_{m-1}$ and $\psi_{F,n}^{(m,r)}(x_m)=1$ and $\psi_{F,n}^{(m,l)}(x_m)=0$ at $x=x_m$. This will be useful when deriving the VCTMIE. Once the coefficient vectors for the D_y and B_y components are known, all the other field quantities can be derived from Eqs. (A16). For the sake of convenience, we drop the term $\exp(-j\beta z)$ and replace the z-derivative with $-j\beta$. It is common to denote the TE-to-y mode as the h mode and the TM-to-y mode as the e mode. Therefore we will denote k_{ce} $(=k_{cD})$ as the cutoff wavenumber of the e mode and k_{ch} $(=k_{cB})$ as the same for the h mode.

Next, we will consider the relation between the fields inside a particular dielectric slice and the tangential functions on the slice boundaries. The advantage of using $\psi_F^{(m,a)}(x)$, with $a=l,r$, and $F=B,D$ functions becomes clear when we evaluate $E_y(x,y)$ and $H_y(x,y)$ functions on the slice boundaries $(x=x_m)$ $(m=1,2,\ldots,M)$; only one of the unknown coefficient vectors $c_F^{(m,a)}$ is used. Combining this with the orthogonality conditions of the slice basis functions $\{\phi_{D,n}^{(m)}(y)\}$ and $\{\phi_{B,n}^{(m)}(y)\}$, the expansion coefficients can be obtained directly via the following integrals:

$$c_{D,n}^{(m,l)}=\frac{\int \mathcal{E}_{m-1}(y)[\phi_{D,n}^{(m)}(y)]^*\mathrm{d}y}{\int \phi_{D,n}^{(m)}(y)\dfrac{1}{\epsilon_r^{(m)}(y)}[\phi_{D,n}^{(m)}(y)]^*\mathrm{d}y},$$

$$c_{B,n}^{(m,l)}=\frac{\int \mathcal{H}_{m-1}(y)[\phi_{B,n}^{(m)}(y)]^*\mathrm{d}y}{\int \phi_{B,n}^{(m)}(y)[\phi_{B,n}^{(m)}(y)]^*\mathrm{d}y}, \tag{6a}$$

$$c_{D,n}^{(m,r)}=\frac{\int \mathcal{E}_{m}(y)[\phi_{D,n}^{(m)}(y)]^*\mathrm{d}y}{\int \phi_{D,n}^{(m)}(y)\dfrac{1}{\epsilon_r^{(m)}(y)}[\phi_{D,n}^{(m)}(y)]^*\mathrm{d}y},$$

$$c_{B,n}^{(m,r)}=\frac{\int \mathcal{H}_{m}(y)[\phi_{B,n}^{(m)}(y)]^*\mathrm{d}y}{\int \phi_{B,n}^{(m)}(y)[\phi_{B,n}^{(m)}(y)]^*\mathrm{d}y}. \tag{6b}$$

Further assuming that these basis functions are also normalized, the denominators in Eqs. (6a) and (6b) become unity and will be omitted from here on. Note that there is only one term in $c_{D,n}^{(m)}$ and $c_{B,n}^{(m)}$ in the first and the last slice. Substituting Eqs. (6) into Eqs. (2) and (3), we can represent $D_y(x,y)$ in terms of the interfacial field function $\mathcal{E}(y)$ as

$$D_y^{(m)}(x,y)=\sum_n \phi_{D,n}^{(m)}(y)\left\{\int \mathcal{E}_{(m-1)}(y')[\phi_{D,n}^{(m)}(y')]^*\mathrm{d}y'\psi_{D,n}^{(m,l)}(x)+\int \mathcal{E}_m(y')[\phi_{D,n}^{(m)}(y')]^*\mathrm{d}y'\psi_{D,n}^{(m,r)}(x)\right\}, \tag{7}$$

and similarly $B_y(x,y)$ in terms of $\mathcal{H}(y)$ as

$$B_y^{(m)}(x,y)=\sum_n \phi_{B,n}^{(m)}(y)\left\{\int \mathcal{H}_{m-1}(y')[\phi_{B,n}^{(m)}(y')]^*\mathrm{d}y'\psi_{D,n}^{(m,l)}(x)+\int \mathcal{H}_m(y')[\phi_{B,n}^{(m)}(y')]^*\mathrm{d}y'\psi_{D,n}^{(m,r)}\right\}. \tag{8}$$

Note that in the first $(m=1)$ and the last slice $(m=M+1)$, only one term is needed for the previous two equations. To make the symbols short and easy to recognize, we define the upper case Φ to represent the derivative of ϕ with respect to y such that

$$\Phi_D(y)=\frac{1}{\epsilon_r(y)}\frac{\mathrm{d}[\phi_D(y)]}{\mathrm{d}y},\quad \Phi_B(y)=\frac{1}{\mu_r}\frac{\mathrm{d}[\phi_B(y)]}{\mathrm{d}y}. \tag{9}$$

Similarly, the symbol Ψ is the derivative of ψ with respect to x. For example, within the slices $2\leqslant m\leqslant M$, $\Psi_{F,n}^{(m)}$ with $F=B,D$ can be shown as

$$\Psi_{F,n}^{(m,l)}(x)=\frac{\mathrm{d}}{\mathrm{d}x}[\psi_{F,n}^{(m,l)}(x)]=\frac{-k_{xF,n}^{(m)}\cos[k_{xF,n}^{(m)}(x_m-x)]}{\sin[k_{xF,n}^{(m)}\Delta x_m]}, \tag{10a}$$

$$\Psi_{F,n}^{(m,r)}(x)=\frac{\mathrm{d}}{\mathrm{d}x}[\psi_{F,n}^{(m,r)}(x)]=\frac{-k_{xF,n}^{(m)}\cos[k_{xF,n}^{(m)}(x-x_{m-1})]}{\sin[k_{xF,n}^{(m)}\Delta x_m]}. \tag{10b}$$

So far we are able to express $D_y(x,y)$ and $B_y(x,y)$ in terms of the unknown interfacial functions $\mathcal{E}(y)$ and $\mathcal{H}(y)$. Next, we wish to derive in the same manner expressions for the z-component EM fields that will be used to set up the equations for the unknown functions $\mathcal{E}(y)$ and $\mathcal{H}(y)$. We substitute Eqs. (2a) and (3a) into Eq. (A16b) and get

$$E_z^{(1)}(x,y) = \frac{-j\beta}{[k_{ce,n}^{(1)}]^2\epsilon^{(1)}(y)}\frac{\partial D_y^{(1)}}{\partial y} - \frac{j\omega}{[k_{ch,n}^{(1)}]^2}\frac{\partial B_y^{(1)}}{\partial x}$$
$$= \int \mathbb{G}_{ee}^{(1,r)}(x,y;y')\mathcal{E}_1(y')\mathrm{d}y' + \int \mathbb{G}_{e,h}^{(1,r)}(x,y;y')\mathcal{H}_1(y')\mathrm{d}y', \quad (11a)$$

where the Green's functions to produce $E_z(x,y)$ can be written as

$$\mathbb{G}_{ee}^{(1,r)}(x,y;y') = \sum_n \frac{-j\beta}{[k_{ce,n}^{(1)}]^2}\psi_{D,n}^{(1,r)}(x)\Phi_{D,n}^{(1)}(y)[\phi_{D,n}^{(1)}(y')]^*, \quad (11b)$$

$$\mathbb{G}_{eh}^{(1,r)}(x,y;y') = \sum_n \frac{-j\omega}{[k_{ch,n}^{(1)}]^2}\Psi_{B,n}^{(1,r)}(x)\phi_{B,n}^{(1)}(y)[\phi_{B,n}^{(1)}(y')]^*. \quad (11c)$$

In the expression above, the asterisk (*) denotes the complex conjugate. We use the open font to represent the kernels of the integral operators. The first and the second superscript of the Green's function $\mathbb{G}_{ee}^{(1,r)}$ denote the destination and the source locations, respectively, while the first and the second subscript denote target component $E_z^{(1)}$ and source polarization $\mathcal{E}(y)$, respectively. $\mathbb{G}_{eh}^{(1,r)}$ is the operator that maps the interfacial function $\mathcal{H}(y)$ on the right side toward the electric field $E_z^{(1)}$ in the first slice. Both Green's functions are functions of x and y. Similarly, substituting Eqs. (2a) and (3a) into Eq. (A16d), we obtain the z-component magnetic field intensity $H_z^{(1)} \times (x,y)$ as

$$H_z^{(1)}(x,y) = \frac{j\omega}{[k_{ce,n}^{(1)}]^2}\frac{\partial D_y^{(1)}}{\partial x} + \frac{-j\beta}{[k_{ch,n}^{(1)}]^2\mu^{(1)}(y)}\frac{\partial B_y^{(1)}}{\partial y}$$
$$= \int \mathbb{G}_{he}^{(1,r)}(x,y;y')\mathcal{E}_1(y')dy' + \int \mathbb{G}_{hh}^{(1,r)}(x,y;y')\mathcal{H}_1(y')dy', \quad (12a)$$

where the Green's function of H_z can be written as

$$\mathbb{G}_{he}^{(1,r)}(x,y;y') = \sum_n \frac{j\omega}{[k_{ce,n}^{(1)}]^2}\Psi_{D,n}^{(1,r)}(x)\phi_{D,n}^{(1)}(y)[\phi_{D,n}^{(1)}(y')]^*, \quad (12b)$$

$$\mathbb{G}_{hh}^{(1,r)}(x,y;y') = \sum_n \frac{-j\beta}{[k_{ch,n}^{(1)}]^2}\psi_{B,n}^{(1,r)}(x)\Phi_{B,n}^{(1)}(y)[\phi_{B,n}^{(1)}(y')]^*. \quad (12c)$$

The meanings of these Green's function $\mathbb{G}_{he}^{(1,r)}$ and $\mathbb{G}_{hh}^{(1,r)}$ follow the same rules as for $\mathbb{G}_{ee}^{(1,r)}$ and $\mathbb{G}_{ee}^{(1,r)}$. Combining Eqs. (11) and Eqs. (12), we get the following matrix form:

$$\begin{bmatrix} H_z^{(1)}(x,y) \\ E_z^{(1)}(x,y) \end{bmatrix} = \int \mathrm{d}y' \begin{bmatrix} \mathbb{G}_{he}^{(1,r)}(x,y;y') & \mathbb{G}_{hh}^{(1,r)}(x,y;y') \\ \mathbb{G}_{ee}^{(1,r)}(x,y;y') & \mathbb{G}_{eh}^{(1,r)}(x,y;y') \end{bmatrix} \times \begin{bmatrix} \mathcal{E}_1(y') \\ \mathcal{H}_1(y') \end{bmatrix}. \quad (13)$$

The z-component fields approaching the first interface inside the first slice from the left side can be written as

$$\begin{bmatrix} H_z^{(1)}(x_1-\delta,y) \\ E_z^{(1)}(x_1-\delta,y) \end{bmatrix} = \int \mathrm{d}y' \begin{bmatrix} \mathbb{R}_{he}^{(1)}(y,y') & \mathbb{R}_{hh}^{(1)}(y,y') \\ \mathbb{R}_{ee}^{(1)}(y,y') & \mathbb{R}_{eh}^{(1)}(y,y') \end{bmatrix} \begin{bmatrix} \mathcal{E}_1(y') \\ \mathcal{H}_1(y') \end{bmatrix}, \quad (14)$$

where the kernels $\mathbb{R}_{uv}^{(1)}$, $u, v = e,h$ are obtained by evaluating $\mathbb{G}_{uv}^{(1,r)}$ at $x = x_1$ and are given by

$$\mathbb{R}_{he}^{(1)}(y,y') = \sum_h \frac{j\omega}{[k_{ce,n}^{(1)}]^2}\Psi_{D,n}^{(1,r)}(x_1)\phi_{D,n}^{(1)}(y)[\phi_{D,n}^{(1)}(y')]^*, \quad (15a)$$

$$\mathbb{R}_{hh}^{(1)}(y,y') = \sum_n \frac{-j\beta}{[k_{ch,n}^{(1)}]^2}\psi_{B,n}^{(1,r)}(x_1)\Phi_{B,n}^{(1)}(y)[\phi_{B,n}^{(1)}(y')]^*, \quad (15b)$$

$$\mathbb{R}_{ee}^{(1)}(y,y') = \sum_n \frac{-j\beta}{[k_{ce,n}^{(1)}]^2}\psi_{D,n}^{(1,r)}(x_1)\Phi_{D,n}^{(1)}(y)[\phi_{D,n}^{(1)}(y')]^*, \quad (15c)$$

$$\mathbb{R}_{eh}^{(1)}(y,y') = \sum_n \frac{-j\omega}{[k_{ch,n}^{(1)}]^2}\Psi_{B,n}^{(1,r)}(x_1)\phi_{B,n}^{(1)}(y)[\phi_{B,n}^{(1)}(y')]^*. \quad (15d)$$

Note that in Eq. (14) we deliberately reverse the ordering of the output vector from that of the input vector. This is because in the normal case (scalar mode) H_z is generated by E_y and E_z is generated by H_y. In this order, the diagonal operators will be the dominating terms and the off-diagonal terms will be small or zero in the limiting scalar cases.

We are now able to express the mth slice electric field $E_z^{(m)}(x,y)$ in terms of the four adjacent $\mathcal{E}_{m-1}, \mathcal{E}_m$, and $\mathcal{H}_{m-1}, \mathcal{H}_m$ functions via

$$E_z^{(m)}(x,y) = \int \mathbb{G}_{ee}^{(m,l)}(x,y;y')\mathcal{E}_{m-1}(y')\mathrm{d}y' + \int \mathbb{G}_{eh}^{(m,l)} \times (x,y;y')\mathcal{H}_{m-1}(y')\mathrm{d}y' + \int \mathbb{G}_{ee}^{(m,r)} \times (x,y;y')\mathcal{E}_m(y')\mathrm{d}y' + \int \mathbb{G}_{eh}^{(m,r)}(x,y;y')\mathcal{H}_m(y')\mathrm{d}y', \quad (16a)$$

where the Green's functions are

$$\mathbb{G}_{ee}^{(m,l)}(x,y;y') = \sum_n \frac{-j\beta}{[k_{ce,n}^{(m)}]^2} \psi_{D,n}^{(m,l)}(x)\Phi_{D,n}^{(m)}(y)[\phi_{D,n}^{(m)}(y')]^*, \tag{16b}$$

$$\mathbb{G}_{eh}^{(m,l)}(x,y;y') = \sum_n \frac{-j\omega}{[k_{ch,n}^{(m)}]^2} \Psi_{B,n}^{(m,l)}(x)\phi_{B,n}^{(m)}(y)[\phi_{B,n}^{(m)}(y')]^*, \tag{16c}$$

$$\mathbb{G}_{ee}^{(m,r)}(x,y;y') = \sum_n \frac{-j\beta}{[k_{ce,n}^{(m)}]^2} \psi_{D,n}^{(m,r)}(x)\Phi_{D,n}^{(m)}(y)[\phi_{D,n}^{(m)}(y')]^*, \tag{16d}$$

$$\mathbb{G}_{eh}^{(m,r)}(x,y;y') = \sum_n \frac{-j\omega}{[k_{ch,n}^{(m)}]^2} \Psi_{B,n}^{(m,r)}(x)\phi_{B,n}^{(m)}(y)[\phi_{B,n}^{(m)}(y')]^*. \tag{16e}$$

Similarly, we express the 2D magnetic field $H_z^{(m)}(x,y)$ in the mth slice as

$$H_z^{(m)}(x,y) = \int \mathbb{G}_{he}^{(m,l)}(x,y;y')\mathcal{E}_{m-1}(y')\mathrm{d}y' + \int \mathbb{G}_{hh}^{(m,l)} \times(x,y;y')\mathcal{H}_{m-1}(y')\mathrm{d}y' + \int \mathbb{G}_{he}^{(m,r)} \times(x,y;y')\mathcal{E}_m(y')\mathrm{d}y' + \int \mathbb{G}_{hh}^{(m,r)}(x,y;y')\mathcal{H}_m(y')\mathrm{d}y', \tag{17a}$$

where the Green's functions are

$$\mathbb{G}_{he}^{(m,l)}(x,y;y') = \sum_n \frac{j\omega}{[k_{ce,n}^{(m)}]^2} \Psi_{D,n}^{(m,l)}(x)\phi_{D,n}^{(m)}(y)[\phi_{D,n}^{(m)}(y')]^*, \tag{17b}$$

$$\mathbb{G}_{hh}^{(m,l)}(x,y;y') = \sum_n \frac{-j\beta}{[k_{ch,n}^{(m)}]^2} \psi_{B,n}^{(m,l)}(x)\Phi_{B,n}^{(m)}(y)[\phi_{B,n}^{(m)}(y')]^*, \tag{17c}$$

$$\mathbb{G}_{he}^{(m,r)}(x,y;y') = \sum_n \frac{j\omega}{[k_{ce,n}^{(m)}]^2} \Psi_{D,n}^{(m,r)}(x)\phi_{D,n}^{(m)}(y)[\phi_{D,n}^{(m)}(y')]^*, \tag{17d}$$

$$\mathbb{G}_{hh}^{(m,r)}(x,y;y') = \sum_n \frac{-j\beta}{[k_{ch,n}^{(m)}]^2} \psi_{B,n}^{(m,r)}(x)\Phi_{B,n}^{(m)}(y)[\phi_{B,n}^{(m)}(y')]^*. \tag{17e}$$

Likewise, the z-components of electromagnetic fields at the mth slice interfaces can be written as

$$\begin{bmatrix} H_z^{(m)}(x_{m-1}+\delta,y) \\ E_z^{(m)}(x_{m-1}+\delta,y) \end{bmatrix} = \int \mathrm{d}y' \begin{bmatrix} \mathbb{Q}_{he}^{(m)}(y,y') & \mathbb{Q}_{hh}^{(m)}(y,y') \\ \mathbb{Q}_{ee}^{(m)}(y,y') & \mathbb{Q}_{eh}^{(m)}(y,y') \end{bmatrix} \times \begin{bmatrix} \mathcal{E}_{m-1}(y') \\ \mathcal{H}_{m-1}(y') \end{bmatrix} + \int \mathrm{d}y' \begin{bmatrix} \mathbb{S}_{he}^{(m)}(y,y') & 0 \\ 0 & \mathbb{S}_{eh}^{(m)}(y,y') \end{bmatrix} \times \begin{bmatrix} \mathcal{E}_m(y') \\ \mathcal{H}_m(y') \end{bmatrix}, \tag{18a}$$

$$\begin{bmatrix} H_z^{(m)}(x_m-\delta,y) \\ E_z^{(m)}(x_m-\delta,y) \end{bmatrix} = \int \mathrm{d}y' \begin{bmatrix} \mathbb{P}_{he}^{(m)}(y,y') & 0 \\ 0 & \mathbb{P}_{eh}^{(m)}(y,y') \end{bmatrix} \times \begin{bmatrix} \mathcal{E}_{m-1}(y') \\ \mathcal{H}_{m-1}(y') \end{bmatrix} + \int \mathrm{d}y' \begin{bmatrix} \mathbb{R}_{he}^{(m)}(y,y') & \mathbb{R}_{hh}^{(m)}(y,y') \\ \mathbb{R}_{ee}^{(m)}(y,y') & \mathbb{R}_{eh}^{(m)}(y,y') \end{bmatrix} \times \begin{bmatrix} \mathcal{E}_m(y') \\ \mathcal{H}_m(y') \end{bmatrix}, \tag{18b}$$

Here the open font $\mathbb{P}_{uv}^{(m)}, \mathbb{Q}_{uv}^{(m)}, \mathbb{R}_{uv}^{(m)}, \mathbb{S}_{uv}^{(m)}$ denote sixteen operator kernels that transform the left and right pair of y-directed interfacial functions into the z-directed interfacial functions through the h and e slice modes. They are equal to the eight Green's kernels defined in Eqs. (16b)–(16e) and Eqs. (17b)–(17e) evaluated at $x=x_{m-1}$ and at $x=x_m$, respectively. In this case, we have

$$\mathbb{P}_{uv}^{(m)} = \mathbb{G}_{uv}^{(m,l)}|_{x=x_m}, \quad \mathbb{Q}_{uv}^{(m)} = \mathbb{G}_{uv}^{(m,l)}|_{x=x_{m-1}}, \tag{19}$$

$$\mathbb{R}_{he}^{(m)} = \mathbb{G}_{he}^{(m,l)}|_{x=x_m}, \quad \mathbb{S}_{uv}^{(m)} = \mathbb{G}_{uv}^{(m,r)}|_{x=x_{m-1}}, \tag{20}$$

where the subscript u,v stands for e and h mode, respectively. Note that in Eqs. (18) we have reflected the fact that $\mathbb{P}_{ee}^{(m)}=\mathbb{P}_{hh}^{(m)}=0$ and $\mathbb{S}_{ee}^{(m)}=\mathbb{S}_{hh}^{(m)}=0$ which can be easily verified from Eqs. (19) and (20). The physical significance is that inside a sliced waveguide the y-directed field component does not contribute to the z-directed component on the opposite side if it is of the same polarization. The letter $\mathbb{P}$ is chosen for propagation and $\mathbb{R}$ is chosen for reflection. The letters $\mathbb{Q}$ and $\mathbb{S}$ are chosen for reflection and propagation, respectively, in the opposite direction. To assist in remembering this association, just keep in mind that $\mathbb{Q}$ goes before $\mathbb{R}$, $\mathbb{P}$ goes before $\mathbb{S}$, and "left" goes before "right." So $\mathbb{P}$ is from left to right while $\mathbb{S}$ is from right to left, and $\mathbb{Q}$ is the reflection operator on the left side just as

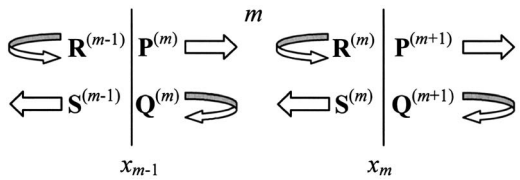

Fig. 2. Definitions of $\mathbf{P},\mathbf{Q},\mathbf{R},\mathbf{S}$ generalized impedance matrices.

$\mathbb{R}$ is the reflection operator on the right side. Figure 2 further illustrates this relationship.

The field expressions of $E_z^{(M+1)}$ and $H_z^{(M+1)}$ for the last slice can be obtained in a similar way. So far, we have derived the fields within all slices in terms of the unknown y-directed functions on the slice boundaries. Next, we will derive the equations that these unknown functions must satisfy. First we consider a simple structure made of two dielectric slices with just one interface. The z-component electromagnetic fields on either side of the interface boundary must be the same for every point on the boundary. From Eqs. (14) and (18), we obtain

$$\int dy' \begin{bmatrix} \mathbb{R}_{he}^{(1)}(y,y') & \mathbb{R}_{hh}^{(1)}(y,y') \\ \mathbb{R}_{ee}^{(1)}(y,y') & \mathbb{R}_{eh}^{(1)}(y,y') \end{bmatrix} \begin{bmatrix} \mathcal{E}_1(y') \\ \mathcal{H}_1(y') \end{bmatrix} = \int dy' \begin{bmatrix} \mathbb{Q}_{he}^{(2)}(y,y') & \mathbb{Q}_{hh}^{(2)}(y,y') \\ \mathbb{Q}_{ee}^{(2)}(y,y') & \mathbb{Q}_{eh}^{(2)}(y,y') \end{bmatrix} \begin{bmatrix} \mathcal{E}_1(y') \\ \mathcal{H}_1(y') \end{bmatrix}. \quad (21)$$

We can further simplify this equation by upgrading the four open-font symbols $\mathbb{P},\mathbb{Q},\mathbb{R},\mathbb{S}$ into bold face letters $\mathbf{P},\mathbf{Q},\mathbf{R},\mathbf{S}$ which, in this paper, represent the matrices. Thus Eq. (21) becomes

$$\int dy' [\mathbf{R}^{(1)} - \mathbf{Q}^{(2)}]\mathbf{F}_1 = 0, \quad (22)$$

where $\mathbf{F}_i$ is the vector of the unknown functions as

$$\mathbf{F}_i = \begin{bmatrix} \mathcal{E}_i(y') \\ \mathcal{H}_i(y') \end{bmatrix}, \quad i = 1,2,\ldots,M. \quad (23)$$

Let $\mathbf{A}$ be one of the $\mathbf{P},\mathbf{Q},\mathbf{R},\mathbf{S}$ matrices organized as

$$\mathbf{A}^{(m)} = \begin{bmatrix} \mathbb{A}_{he}^{(m)} & \mathbb{A}_{hh}^{(m)} \\ \mathbb{A}_{ee}^{(m)} & \mathbb{A}_{eh}^{(m)} \end{bmatrix}. \quad (24)$$

For the complex RWG structure with more than two interfaces, we can obtain the banded general VCTMIE as the matrix equation

$$\int dy' \begin{bmatrix} [\mathbf{R}^{(1)} - \mathbf{Q}^{(2)}] & -\mathbf{S}^{(2)} & 0 & \cdots & 0 \\ \mathbf{P}^{(2)} & [\mathbf{R}^{(2)} - \mathbf{Q}^{(3)}] & -\mathbf{S}^{(3)} & 0 & \vdots \\ 0 & \ddots & \ddots & \ddots & 0 \\ \vdots & \ddots & \mathbf{P}^{(M-1)} & [\mathbf{R}^{(M-1)} - \mathbf{Q}^{(M)}] & -\mathbf{S}^{(M)} \\ 0 & \cdots & 0 & \mathbf{p}^{(M)} & [\mathbf{R}^{(M)} - \mathbf{Q}^{(M+1)}] \end{bmatrix} \begin{bmatrix} \mathbf{F}_1 \\ \mathbf{F}_2 \\ \vdots \\ \mathbf{F}_{M-1} \\ \mathbf{F}_M \end{bmatrix} = 0. \quad (25)$$

Note that the sub matrices $\mathbf{P}^{(m)}$ and $-\mathbf{S}^{(m)}$ are equal to each other due to the symmetry of the propagation matrices. Using the notations defined in Eqs. (23) and (24), we have arrived at Eq. (25) with a tridiagonal matrix structure that looks like those derived for the scalar case. In other words, the unknown vector functions are related to their two nearby neighbors. Each boldface symbol on the diagonal represents a full 2×2 operator matrix, while the off-diagonal symbols $\mathbf{P}^{(m)}$ and $\mathbf{S}^{(m)}$ are 2×2 diagonal matrices. We conclude that the final matrix in Eq. (25) is actually a banded matrix of a bandwidth equal to 5. In part II[18] we will continue the discussion of the numerical methods for solving Eq. (25) as well as discussion of various waveguide examples computed by this VCTMIE formulation.

3. DISCUSSION

A. Continuity Properties of Electromagnetic Field Components within the Slice Waveguides

In the left and right columns of Fig. 3, we compare the fundamental mode field profiles between h and e modes inside a 1D dielectric slab waveguide with distinct core and cladding indices. Since these are the basic building blocks for the full-vector solutions of 2D ridged waveguides, we will carefully examine the continuity properties of these components. We note first that inside the slab waveguide, the vertical electric field intensity component $E_y(y)$ jumps at the core–cladding interface, while all other components are continuous. Inside the slab waveguide, $E_x(y),E_z(y)$, being the tangential components, are by default continuous. The normal flux components, including the displacement current $D_y(y)$ and the magnetic flux density $B_y(y)$, are also continuous across the interface. However, the continuity properties of their first- and second-order derivatives are not clear from the figure. For example, $\partial E_y/\partial y$ is the same (except at the index boundary) as $[1/\epsilon_r(y)]\partial D_y/\partial y$, which is linearly related to E_x,E_z. We conclude that the two-sided normal derivative of E_y is continuous.

As for the four transverse EM components E_x,E_z,H_x,H_z we turn to the generating Eqs. (A16), remembering that all partial derivatives with respect to x and z are the same for all layers. Thus, if a function is continuous then also are all its higher-order derivatives with respect to the x and z axes. The first normal derivative of the e mode's E_x,E_z components and the h mode's H_x,H_z components are linearly related to the second-order normal derivative of D_y and B_y. By Eqs. (A13a) and (A13b) they are related to $n^2(y)k_0^2\times(D_y/B_y)$ and are therefore discontinuous. We may also apply similar arguments to get the continuity properties of the second-order derivatives of these functions since they determine the concavity of the curves. In particular, we know that for a guiding mode, the square of the transverse propagation constant $\beta^2+k_{xF}^2$ is between $n_0^2k_0^2$ and $n_1^2k_0^2$; this will pro-

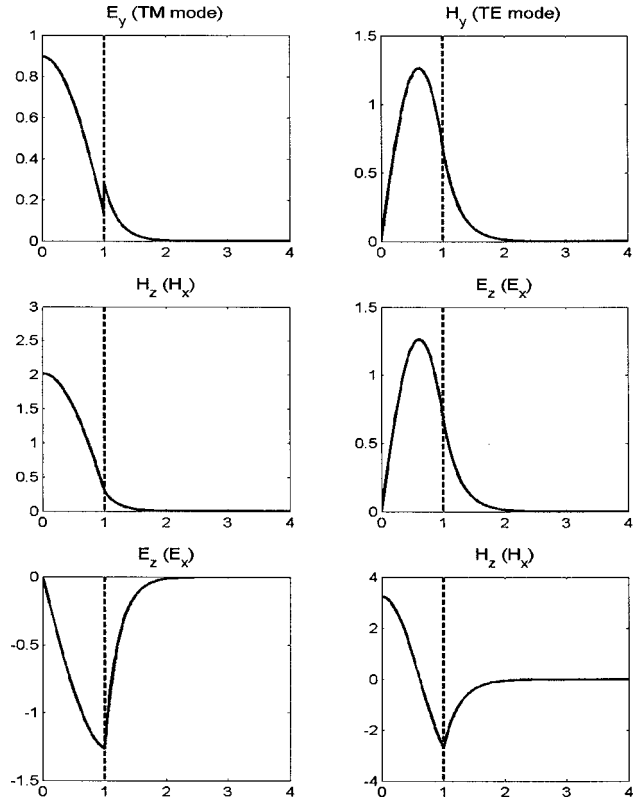

Fig. 3. Fundamental mode field components of TE-to-y and TM-to-y modes for a slab waveguide. The x coordinate is in micrometers, while the y coordinate represents relative field intensity. Due to symmetry, only half the figures (positive x) are shown. $\lambda = 1.5\ \mu$m, $n_1 = 1.5$, $n_0 = 1.0$, $d = 1$.

duce a sign change in the second derivatives of the bottom curves of Fig. 3 when the condition is applied to Eqs. (A13) and (A14). The second derivatives of all other components retain the same sign.

B. Fields around the Dielectric Corners

It is known that the EM field near a right-angle dielectric corner can be quite complex and tricky.[24] Generally speaking, E_t, D_n are continuous across dielectric interfaces; therefore, E_n and D_t become discontinuous in a step-index medium. The unknown interfacial functions $\mathcal{E}_y(y)$ and $\mathcal{H}_y(y)$ are continuous across slices. Yet the same $E_y(x,y)$ becomes discontinuous once it is inside the inhomogeneous slice as it becomes a normal component. We know that when a discontinuous function is expanded in terms of a set continuous basis, the series representation of the discontinuous function will overshoot (sometimes as much as 10%) and will oscillate around the points of discontinuity. Moreover, as we increase the upper summation limit, the overshots and the oscillation will not die down; we see only the shrinking of the problematic region. This is the well-known Gibb's phenomenon.[25] We will discuss this further and give detailed numerical examples in part II.[18]

C. VCTMIE Formulation without Using Perfectly Conducting Walls

In our VCTMIE formulation for 2D complex dielectric waveguides we place a PCW on the top and bottom of the structure. For waveguides with certain symmetry this is exactly what we want so that we may reduce the domain of the problem and cut down the computational costs. For open dielectric structures, the use of PCWs becomes an approximation. For an unbounded multilayered waveguide, the modes are composed in terms of both discrete guiding modes and continuous radiation modes.[26] The sixteen PQRS operators will be modified to include a finite summation term for the discrete spectrum and an integral term (with the upper limit extended to infinity) for the continuous spectrum. In doing so, we not only make the formulation more complex than it already is but also impose a very difficult task for numerical implementation of the VCTMIE. Without an exact formula, an integral must be evaluated numerically by discrete sum using, say, the Gaussian quadrature. Any such numerical integration method is essentially a discretization process that generates a set of nonorthogonal functions. The unknown expansion coefficient vectors can no longer be written explicitly as in Eqs. (6a). Thus the integral equation can not be derived. VCTMIE formulation for the open structures will be less useful for numerical purposes.

D. Comparison with the Film-Mode-Matching Method

Among various methods of dealing with vectorial modal solutions of RWGs, the FMM structure resembles that of the VCTMIE method most closely. The main difference is that the FMM lacks the exact integral equation and the resulting benefit from the new formulation, such as the flexibility of choosing arbitrary expansion bases for the unknown vertical tangential fields $\mathcal{E}_y$ and $\mathcal{H}_y$. Unknowns in the FMM method are the coefficient vectors of slice modes in each slice section, whereas in VCTMIE the unknowns are interfacial field functions. In the FMM example, a rectangular waveguide was analyzed by simultaneous mode-matching along the slice interface with the y- and z-components of electric and magnetic fields with a finite number of slice modes [$N^{(m)}$ modes for each region/polarization] from slices I and II. The advantages of FMM are the easy comprehension of the mode-matching principle and its superior computational efficiency in which very accurate waveguide propagation constants can be obtained with relatively few slice modes. However, many more slice modes are needed, along with larger matrices, to compute accurate field solutions and minimize the artificial discontinuity in the homogeneous regions of vector fields across the slice interfaces. Under the VCTMIE formulation, the unknown interfacial $\mathcal{E}_y(y)$ and $\mathcal{H}_y(y)$ functions can be efficiently expressed in terms of some optimized basis functions with fewer terms [$N_b^{(m)}$ terms for each interface/polarization]. We then use as many slice modes as are needed [$N^{(m)} \approx 5N_b^{(m)}$] to match the chosen basis functions. As a result, vector fields across the slice interfaces become continuous in the homogeneous regions, and the Gibb's phenomenon at the dielectric corners is greatly reduced (see Part II,[18] Fig. 7). If we choose the interfacial basis functions to be one of the slice modes and keep the number of terms in PQRS operators all the same, the final coupled matrix equation will be the same as those obtained by FMM. The two methods are then identical.

The advantage of VCTMIE is that the size of the nonlinear matrix equation remains unchanged while the costs of computing the additional slice modes and the final matrix increase only linearly with respect to the total number of slice modes used in each region (see Part II,[18] Eq. (18)). Both FMM and VCTMIE methods are dependent on the capability of constructing complete 1D layer modes of given complex dielectric slab waveguides, which is hard to do in the case of a structure with nearly degenerate modes. Finally, we wish to point out that there are other ways to solve the VCTMIE that are otherwise not available to FMM. For example, using approximate solutions to the unknown $\mathcal{E}_y(y)$ and $\mathcal{H}_y(y)$ functions (via some effective-index method or some iterative solutions), all the mode field solutions can be obtained with Eqs. (6)–(8).

4. CONCLUSION

In this paper, we have constructed a rigorous VCTMIE formulation to study modal characteristics of rectangular-pattern dielectric waveguides as commonly found in integrated optical circuits. In this vector formulation, a RWG is first approximated by a collection of dielectric slices. Within each slice the 4×4 kernel matrix constructed from both TE-to-y and TM-to-y modes map the unknown y-directed interfacial functions on the slice boundaries onto the z-component electric and magnetic fields. The continuity of these z-directed EM field components along each slice interface provide governing integral equations on the unknown interfacial functions $\mathcal{E}_y$ and $\mathcal{H}_y$. To solve the unknown functions, we construct sets of suitable expansion functions and turn VCTMIE into an optimized matrix equation. We leave the verification of our formulation as well as detailed numerical discussion to part II.[18]

APPENDIX A: DERIVATION OF THE TE-y AND TM-y STURM–LIOUVILLE FORM

For 1D dielectric layered media, we obtain from time-harmonic Maxwell's equations

$$\frac{1}{\mu_0}\nabla\times\left[\frac{1}{j\omega\epsilon_0\epsilon_r(y)}\nabla\times\bar{B}\right]=-j\omega\bar{B}. \tag{A1}$$

$\epsilon_r(y)$ is the relative permittivity and μ_0 is assumed in all regions, and they are dropped for simplicity. Using the vector identity

$$\nabla\times(\phi\bar{A})=\nabla\phi\times\bar{A}+\phi\nabla\times\bar{A}$$

and

$$\nabla\cdot\vec{B}=0, \tag{A2}$$

Eq. (A1) can be rewritten as

$$\nabla^2\bar{B}+k_0^2\epsilon_r(y)\bar{B}-\epsilon_r(y)\nabla\frac{1}{\epsilon_r(y)}\times(\nabla\times\bar{B})=0. \tag{A3}$$

Note that the term $\nabla[1/\epsilon_r(y)]$ has only the y component, and the result after the curl operation will not produce any y component. Therefore, the resulting differential equation for the y component of the magnetic field in Eq. (A3) is

$$\nabla^2B_y+k_0^2\epsilon_r(y)B_y=0. \tag{A4}$$

We seek the solution in the following form:

$$B_y(x,y,z)=\phi_B(y)\exp(-jk_{xB}x)\exp(-j\beta z). \tag{A5}$$

Thus Eq. (A4) can be written as the following differential equation in Sturm–Liouville (S-L) form:

$$[\phi_B'(y)]'+k_0^2\epsilon_r(y)\phi_B(y)=(\beta^2+k_{xB}^2)\phi_B(y). \tag{A6}$$

Next, we seek to find the differential equation for the TM-to-y case. We have

$$\mu_0\nabla\times\left[\frac{1}{\mu_0}\nabla\times\bar{E}\right]=k_0^2\epsilon_r(y)\bar{E}. \tag{A7}$$

Applying the vector identity for the double curls, we obtain

$$\nabla(\nabla\cdot\bar{E})-\nabla^2\bar{E}=k_0^2\epsilon_r(y)\bar{E}. \tag{A8}$$

Using $\nabla\cdot(\bar{D}/\epsilon)=\nabla(1/\epsilon)\cdot\bar{D}+(1/\epsilon)\nabla\cdot\bar{D}$, along with Gauss's law $\nabla\cdot\bar{D}=\rho_s=0$, we can rewrite Eq. (A8) as

$$\nabla^2\frac{\bar{D}}{\epsilon_r(y)}-\nabla\left[\frac{\epsilon_r'(y)}{E_r^2(y)}D_y\right]+k_0^2\bar{D}=0. \tag{A9}$$

Finally equating the y component in Eq. (A9), we get

$$\nabla^2\frac{D_y}{\epsilon_r(y)}+\left[\frac{\epsilon_r'(y)}{\epsilon_y^2(y)}D_y\right]'+k_0^2D_y=0. \tag{A10}$$

Similar to Eq. (A5), we set

$$D_y(x,y,z)=\phi_D(y)\exp(-jk_{xD}x)\exp(-j\beta z). \tag{A11}$$

Substituting Eq. (A11) into Eq. (A10) and after a few algebraic manipulations, we get

$$\left[\frac{\phi_D'(y)}{\epsilon_r(y)}\right]'+k_0^2\phi_D(y)=(\beta^2+k_{xD}^2)\frac{\phi_D(y)}{\epsilon_r(y)}. \tag{A12}$$

Rewriting Eqs. (A6) and (A12) in the standard S-L form, we have

$$L_B[\phi_B(y)]=\phi_B''(y)+k_0^2\epsilon_r(y)\phi_B(y)=\lambda_B\phi_B(y), \tag{A13a}$$

$$L_D[\phi_D(y)]=\left[\frac{\phi_D'(y)}{\epsilon_r(y)}\right]'+k_0^2\phi_D(y)=\lambda_D\frac{\phi_D(y)}{\epsilon_r(y)}, \tag{A13b}$$

where

$$\lambda_B=k_{cB}^2=\beta^2+k_{xB}^2=\epsilon_r(y)k_0^2-k_{yB}^2(y), \tag{A14a}$$

$$\lambda_D=k_{cD}^2=\beta^2+k_{xD}^2=\epsilon_r(y)k_0^2-k_{yD}^2(y). \tag{A14b}$$

In the above equations k_{cB}^2 (TE) and k_{cD}^2 (TM) are the eigenvalues of the 1D slab waveguide for TE-to-y and TM-to-y modes. Equations (A13) and (A14) also give the equation for the vertical wavenumbers $k_{yB}(y)$ (TE) and $k_{yD}(y)$ (TM). They are piecewise-constant functions determined by the eigenvalues of the particular polarization/mode and the optical index within a given layer. On the other

hand, the horizontal transverse wavenumbers k_{xD}, k_{xB}, such as the propagation constant β, remain constant within the entire slab structure for a given wavelength and mode order. From S-L theory,[7] the solutions to Eqs. (A13) $\phi_{B,n}(y)/\phi_{D,n}(y)$ are orthogonal eigenfunctions that can be normalized such that

$$\int \phi_{B,m}(y)\phi_{B,n}(y)\mathrm{d}y = \delta_{m,n}, \tag{A15a}$$

$$\int \frac{\phi_{D,m}(y)\phi_{D,n}(y)}{\epsilon(y)}\mathrm{d}y = \delta_{m,n}, \tag{A15b}$$

where $\delta_{m,n}$ is the Kronecker delta.

Given $D_y(x,y,z)$ and $B_y(x,y,z)$, the remaining four EM components can be obtained from the electromagnetic theory as follows:

$$E_x = \frac{1}{k_{cB}^2\epsilon_r(y)}\frac{\partial^2 D_y}{\partial x \partial y} + \frac{j\omega}{k_{cD}^2}\frac{\partial B_y}{\partial z}, \tag{A16a}$$

$$E_z = \frac{1}{k_{cB}^2\epsilon_r(y)}\frac{\partial^2 D_y}{\partial z \partial y} - \frac{j\omega}{k_{cD}^2}\frac{\partial B_y}{\partial x}, \tag{A16b}$$

$$H_x = \frac{-j\omega}{k_{cB}^2}\frac{\partial D_y}{\partial z} + \frac{1}{k_{cD}^2\mu_r}\frac{\partial^2 B_y}{\partial x \partial y}, \tag{A16c}$$

$$H_z = \frac{j\omega}{k_{cB}^2}\frac{\partial D_y}{\partial x} + \frac{1}{k_{cD}^2\mu_r}\frac{\partial^2 B_y}{\partial z \partial y}. \tag{A16d}$$

ACKNOWLEDGMENTS

The authors thank Yun-Hsien Chang for his technical editing assistance, and the National Science Council of Taiwan for financial support under contracts NSC93-2215-E-110-007 and NSC 94-2215-E-110-012. Financial support was also received from the Ministry of Education Program for Promoting Academic Excellence of Universities under grant 91-E-FA08-1-4.

Corresponding author H.-W. Chang's e-mail address is hchang@mail.nsysu.edu.tw.

REFERENCES

1. E. A. Marcatili, "Dielectric rectangular waveguide and dielectric coupler for integrated optics," Bell Syst. Tech. J. **48**, 2071–2103 (1969).
2. Y. H. Cheng and W. G. Lin, "Investigation of rectangular dielectric waveguides: an iteratively equivalent index method," IEE Proc.: Optoelectron. **137**, 323–329 (1990).
3. J. S. Lee and S. Y. Shin, "On the validity of the effective-index method for rectangular dielectric waveguides," J. Lightwave Technol. **11**, 1320–1324 (1993).
4. Y. Cai, T. Mizumoto, and Y. Naito, "Improved perturbation feedback method for the analysis of rectangular dielectric waveguides," J. Lightwave Technol. **9**, 1231–1237 (1991).
5. J. E. Goell, "A circular-harmonic computer analysis of rectangular dielectric waveguides," Bell Syst. Tech. J. **48**, 2133–2160 (1969).
6. R. Mittra, Y. L. Hou, and V. Jannejad, "Analysis of open dielectric waveguides using mode-matching technique and variational methods," IEEE Trans. Microwave Theory Tech. **28**, 36–43 (1980).
7. S. T. Peng and A. A. Oliner, "Guidance and leakage properties of a class of open dielectric waveguides: part I—mathematical formulations," IEEE Trans. Microwave Theory Tech. **29**, 843–855 (1981).
8. E. W. Kolk, N. H. G. Baken, and H. Blok, "Domain integral equation analysis of integrated optical channel and ridged waveguides in stratified media," J. Lightwave Technol. **38**, 78–85 (1990).
9. H. Y. Yang, J. A. Castaneda, and N. G. Alexopoulos, "An integral equation analysis of an infinite array of rectangular dielectric waveguides," IEEE Trans. Microwave Theory Tech. **38**, 873–880 (1990).
10. K. Sabetfakhri and L. P. B. Katehi, "An integral transform technique for analysis of planar dielectric structures," IEEE Trans. Microwave Theory Tech. **42**, 1052–1062 (1994).
11. G. Athanasoulias and N. K. Uzunoglu, "An accurate and efficient entire-domain basis Galerkin's method for the integral equation analysis of integrated rectangular dielectric waveguides," IEEE Trans. Microwave Theory Tech. **43**, 2794–2804 (1995).
12. V. A. Kalinin and B. K. J. C. Nauwelaers, "Free space dyadic Green's function applied to the full-wave numerical analysis of planar transmission lines and dielectric waveguides," IEE Proc., Part H: Microwaves, Antennas Propag. **143**, 328–334 (1996).
13. T. Rasmussen, J. H. Povlsen, A. Bjarklev, O. Lumholt, B. Pedersen, and K. Rottwitt, "Detailed comparison of two approximate methods for the solution of the scalar wave equation for a rectangular optical waveguide," J. Lightwave Technol. **11**, 429–433 (1993).
14. U. Rogge and R. Pregla, "Method of lines for the analysis of dielectric waveguides," J. Lightwave Technol. **11**, 2015–2020 (1993).
15. R. Scarmozzino, A. Gopinath, R. Pregla, and S. Helfert, "Numerical techniques for modeling guided wave photonic devices," IEEE J. Sel. Top. Quantum Electron. **6**, 150–162 (2000).
16. A. S. Sudbo, "Film mode matching: a versatile numerical method for vector mode field calculations in dielectric waveguides," Pure Appl. Opt. **2**, 211–233 (1993).
17. A. S. Sudbo, "Improved formulation of film mode matching method for mode field calculations in dielectric waveguides," Pure Appl. Opt. **3**, 381–388 (1994).
18. H. W. Chang and T. L. Wu, "Vectorial modal analysis of dielectric waveguides based on coupled transverse-mode integral equation. II. Numerical analysis," J. Opt. Soc. Am. A **23**, 1478–1487 (2006).
19. R. F. Harrington, *Time-Harmonic Electromagnetic Fields* (McGraw-Hill, 1961).
20. A. Ishimaru, *Electromagnetic Propagation, Radiation, and Scattering* (Prentice Hall, 1991).
21. Weng Cho Chew, *Waves and Fields in Inhomogeneous Media* (Van Nostrand Reinhold, 1990).
22. T. L. Wu and H. W. Chang, "Analysis of TE to x and TM to x modes for dielectric slab waveguides," in *Proceedings of Optics and Photonics Taiwan 2001* (National Sun Yat-sen University, 2001), pp. 146–148.
23. T. L. Wu and H. W. Chang, "Guiding mode expansion of a TE and TM transverse-mode integral equation for dielectric slab waveguides with an abrupt termination," J. Opt. Soc. Am. A **18**, 2823–2832 (2001).
24. A. S. Sudbo, "Why are accurate computations of mode fields in rectangular dielectric waveguides difficult?" J. Lightwave Technol. **10**, 418–419 (1992).
25. R. N. Bracewell, *The Fourier Transform and Its Applications* (McGraw-Hill, 2000).
26. T. E. Rozzi, "Rigorous analysis of the step discontinuity in a planar dielectric waveguide," IEEE Trans. Microwave Theory Tech. **26**, 738–746 (1978).